A Facile Synthetic Route to a Family of Mn(III) Monomers and their Structural, Magnetic and Spectroscopic Studies

Jones, Leigh; Barra, Anne-Laure; Ryder, Alan G.; Brechin, Euan K.; Collison, David; Innes, Eric J.L.; Sanz, Sergio; Kelly, Brian; Houton, Edel

European Journal of Inorganic Chemistry

DOI:
10.1002/ejic.201601124

Published: 01/11/2016

Peer reviewed version

FULL PAPER WILEY-VCH

A Facile Synthetic Route to a Family of Mn(III) Monomers and their Structural, Magnetic and Spectroscopic Studies

Edel Houton,[b] Brian Kelly,[b] Sergio Sanz,[c] Eric J. L. McInnes,[e] David Collison,[e] Euan K. Brechin,[c] Anne-Laure Barra,*[d] Alan G. Ryder*[b] and Leigh F. Jones*[a,b]

[a] L. F., Jones
School of Chemistry
Bangor University
Alun Roberts Building, Deiniol Road, Bangor, Wales, UK.
E-mail: leigh.jones@bangor.ac.uk

[b] E. Houton, B. Kelly, A. G. Ryder.
School of Chemistry
NUI Galway
University Road, Galway, Ireland.

[c] S. Sanz, E. K. Brechin.
EaStCHEM School of Chemistry
University of Edinburgh
David Brewster Road, Edinburgh, Scotland.

[d] A.-L. Barra.
LNCMI-CNRS
Grenoble, Cedex, France.

[e] E. J. L. McInnes, D. Collison.
School of Chemistry
University of Manchester
Oxford Road, Manchester, England, UK.

Supporting information for this article is given via a link at the end of the document.

Abstract: We report a rapid and facile synthetic route to the synthesis of a family of Mn(III) monomers of general formula $[Mn(III)F_3(H_2O)(L_{1\text{-}6})]\cdot xH_2O\cdot yMeOH$ (where L_1 = 2,2'-Bipyridyl, x = 2, y = 0 (**1'**); L_2 = 1,10'-Phenanthroline, x = y = 0 (**2'**); L_3 = 6-Methyl-2,2'-dipyridyl, x = y = 0 (**3**), L_4 = 4,4-Dimethyl-2,2'-dipyridyl, x = 2, y = 0 (**4**), L_5 = 5,5'-Dimethyl-2,2'-dipyridyl, x = 0, y = 0.5 (**5**) and L_6 = 5-Chloro-1,10-phenanthroline, x = y = 0 (**6**). Magnetic susceptibility and magnetisation experiments have been employed to elucidate the anisotropic D tensor for each family member (ranging from -3.01 cm^{-1} in **2'** to -4.02 cm^{-1} in **5**), while multi-frequency / high-field EPR spectroscopic measurements and subsequent simulations gave similar values for complexes **1'** (-4.25 cm^{-1}), **2'** (-4.03 cm^{-1}), **4** (-3.90 cm^{-1}) and **5** (-4.04 cm^{-1}). The terminal Mn-F vibrational stretches in **1′-6** have been probed using Raman spectroscopy.

Introduction

Commercially available sources of the Mn(III) ion are relatively scarce and this has connotations for synthetic chemists working in many facets of research.[1] For instance, Mn(III) species are common catalytic reagents[2] in various organic transformations centred on oxidative radical cyclizations,[3] while manganese complexes have been extensively studied as model compounds towards elucidating the function of specific metalloenzymes.[4] Extensive investigations into the beneficial incorporation of F^- anions when acting as a co-catalyst within Pd-catalysed Stille,[5] Suzuki-Miyaura[6] and Hiyama[7] cross-coupling procedures have shown improved catalytic performances due to their triple-role contributions, although control of fluoride ion concentration is required.[7] In the field of molecular magnetism, the Mn(III) ion is an excellent source of single-ion anisotropy and when aggregated into polymetallic cages can often lead to molecules displaying slow relaxation of the magnetisation and magnetic bistability.[8] Synthetic chemists in this field predominantly rely on the redox manipulation of Mn(II), Mn(IV) and Mn(VII) precursors to produce Mn(III) rich polymetallic cages.[9] An alternative, and rather attractive, strategy would be to synthesise new monometallic Mn(III) complexes.

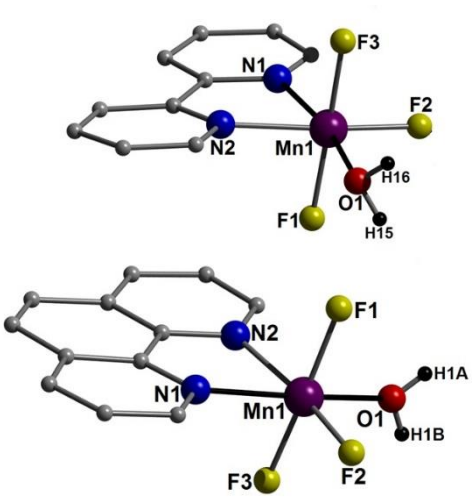

Figure 1. Crystal structures of $[MnF_3(H_2O)(L_1)]\cdot 2H_2O$ (**1′**) (top) and $[MnF_3(H_2O)(L_2)]$ (**2′**) (bottom). Colour code: Purple (Mn), Red (O), Blue (N), Grey (C), Yellow (F) and Black (H).

The strategic incorporation of F-bridges within paramagnetic 3d cages also holds significance in the fields of molecular magnetism and is perhaps best highlighted by the extensive work of Winpenny and co-workers who have developed high yielding synthetic routes to numerous F- bridged Cr(III) complexes, including elegant, extended families of homo- (*i.e.* $[Cr_8]$,[10] $[Cr_9]$[11] and $[Cr_{10}]$[12]) and heterometallic ($[Cr(III)_7M_1]$; M = Ni(II), Co(II), Fe(II), Mn(II), Cd(II))[13] wheels and horseshoes.[14] Examples of F-bridged 3d-4f assemblies were recently presented by Bendix and co-workers when discussing the targeted formation of a family of $[Gd(III)_2M(III)_2]$ molecular magnetic refrigerants (where M = Cr, Fe, Ga from CrF_3, FeF_3 and $GaF_3.3H_2O$ precursors, respectively).[15] With these thoughts in mind, two such examples in the literature caught our eye in the form of the monometallic complexes $[Mn(III)F_3(H_2O)(L)].xH_2O$ (L_1 = 2,2'-Bipyridine, x = 0 (**1**) or L_2 = 1,10'-Phenanthroline, x = 1 (**2**)). These molecules were first synthesised as powders by Chaudhuri *et al*[16] and subsequently characterised crystallographically by the Núñez[17] (**1**) and Rajasekharan[18] (**2**) groups, respectively. Synthesis of these complexes involved the careful handling of toxic 48% HF solutions, requiring manipulation in well ventilated areas. Drawing on our previous experience using anhydrous MnF_3 as a precursor to larger polymetallic architectures,[19] we herein report its utilisation in the synthesis of **1′**$\cdot 2H_2O$ (the hydrated analogue of **1**) and **2′** (the dehydrated analogue of **2**), using a facile reaction route which may be performed in just 5 minutes (Fig. 1). We also demonstrate the robust nature of this synthetic route by describing the formation of their siblings: $[MnF_3(H_2O)(L_3)]$ (**3**), $[MnF_3(H_2O)(L_4)]\cdot 2H_2O$ (**4**), $[MnF_3(H_2O)(L_5)]\cdot 0.5MeOH$ (**5**) and

$[MnF_3(H_2O)(L_6)]$ (**6**) (L_1 = 2,2'-Bipyridyl, L_2 = 1,10'-Phenanthroline, L_3 = 6-Methyl-2,2'-dipyridyl, L_4 = 4,4'-Dimethyl-2,2'-dipyridyl, L_5 = 5,5'-dimethyl-2,2'-dipyridyl and L_6 = 5-Chloro-1,10-phenanthroline) (Fig. 2).

Results and Discussion

The monometallic complexes shown in Figures 1 and 2 were synthesised by heating a methanolic solution of $Mn(III)F_3$ and the appropriate 1,2-diimine ligand (L_x) at 50ºC until a dark red / black colour had formed. Such heating is required to break down and dissolve the extended network structure of MnF_3. Red / orange crystalline solids of **1′-6** subsequently precipitated slowly from the mother liquor, although slow Et_2O diffusion also facilitates X-ray diffraction quality single crystal growth of all complexes. The structures of **1′-6** each comprise a single Jahn-Teller elongated distorted octahedral Mn(III) centre, chelated by a single heterocyclic 1,2-diimine ligand 'L_x', while three terminal F^- ions and a H_2O ligand complete their coordination geometries. The axial distortions in these systems are consistently observed in the form of elongated Mn1-N1 and Mn1-O1 bonds with distances ranging between 2.146 and 2.309 Å, while the shorter terminal Mn-F bonds range from 1.805 to 1.884 Å (Table 1). The remaining Mn1-N2 bond distances range from 2.060 (in **3**) to 2.129 Å (in **4**). Full crystallographic data on all complexes can be found in Tables 2 and 3.

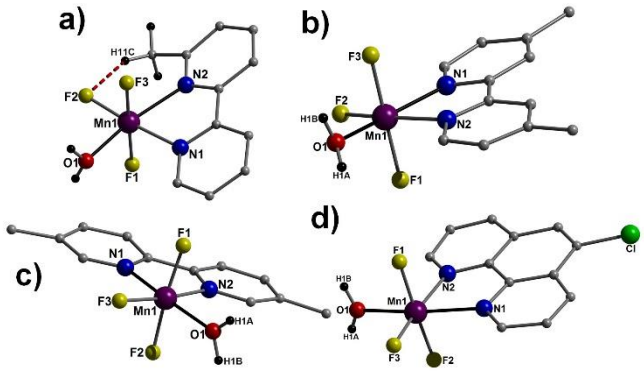

Figure 2. Crystal structures of complexes **3**-**6** (**a-d**), respectively. Colour code as used in Figure 1. Aromatic protons omitted for clarity. Intramolecular H-bond distance in **3** given as dashed red line (C11(H11C)···F2 = 2.232 Å).

The discrete moieties in **1′-3** each pack within their unit cells in a similar manner (Figure 3). The $[MnF_3(H_2O)(L_x)]$ units in each case arrange in superimposable stacks along the *b* direction of their cells. These individual columns of monomeric units arrange along their *ac* planes in an interdigitated fashion with respect to their adjacent rows, forming close contacts primarily in the form of strong H-bonding interactions between the terminal F^- ligands and protons of juxtaposed terminal H_2O ligands (*e.g.* F1···H12′(O1′) = 1.832 Å in **1′**; F1···H1B′(O1′) = 1.878 Å in **2′**, F1···H1H′(O1′) = 1.875 Å in **3**), as well as *via* waters of crystallisation in the case of **1′** (F2···O2 = 2.732 Å and F3···O3′ = 2.792 Å). Secondary interactions are also observed in the form of off-set $\pi_{centroid}\cdots\pi_{centroid}$ stacking interactions (*e.g.*[C1-N5]···[C1′-N5′] = 3.843 Å in **1′**; [C1-N1]···[C4-C12] = 3.784 Å in **2′** and [C6-N2]···[C6′-N2′] = 3.901 Å in **3**). For a list of all intermolecular interactions in **1**-**6** and their corresponding distances see Table S1.

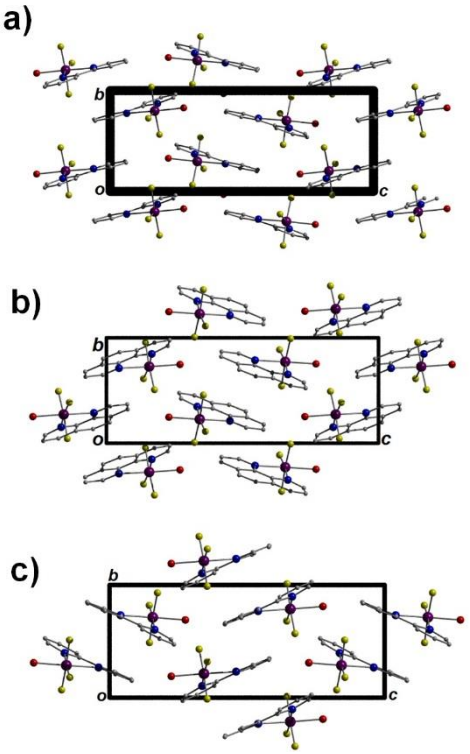

Figure 3. Packing arrays observed in **1′** (a), **2′** (b) and **3** (c) as viewed along the *a* direction of their unit cells. All hydrogen atoms and solvents of crystallisation (in **1′**) have been omitted for clarity. Colour code as used elsewhere in manuscript.

The {Mn} moieties in **4** are linked *via* multiple hydrogen bonding interactions concerning metal bound F^- ligands with nearby H_2O solvents of crystallisation (as in **1**) and not with ligated H_2O moieties as observed in **2′** and **3** (see Table S1 for details). Off-set $\pi_{centroid}\cdots\pi_{centroid}$ arrangements are also forged along the *a* direction of the unit cell in **4** and are separated at a distance of 3.678 Å ([C1-N1]···[C7′-N2′]) (Fig. S1). The packing arrangements in **5** and **6** share similarities in that they both comprise superimposable columns of {Mn} units along the *b* and *a* cell directions, respectively. More specifically these monomers arrange in brickwork sheets (propagating along the *ab* planes in **5** and *ac* plane in **6**) which are held in place by interdigitated off-set $\pi_{centroid}\cdots\pi_{centroid}$ close contacts at distances of 3.886 Å in **5** ([C7-N2]···[C7′-N2′]) and 3.681 Å in **6** ([C1-N1]···[C1′-N1′]). These 2D sheets align in parallel motifs across the *ac* plane in **5** and along the *bc* plane in **6** and are held in position *via* numerous H-

bonding interactions between terminal F^- ions and ligated water protons of juxtaposed monomers (*e.g.* F1···H1B′(O1′) = 1.758 Å in **5** and F1···H1A′(O1′) = 1.766 Å in **6**). Moreover, Cl···F dipole-dipole interactions also influence the overall packing in **6** (F3···Cl1′ = 2.874 Å) and leads to the slight packing differences observed between the two complexes (Fig. S1).

Table 1. Angles and distances concerning the J-T elongation axes in **1′**-**6**.

Complex	J-T elongation distance (Å) (Mn-N and Mn-OH_2)	J-T elongation angle (°) (O-Mn-N)
$[MnF_3(H_2O)(L_1)]\cdot 2H_2O$ (**1′**)	2.220(2); 2.176(2)	168.95
$[MnF_3(H_2O)(L_2)]$ (**2′**)	2.261(2); 2.166(2)	166.99
$[MnF_3(H_2O)(L_3)]$ (**3**)	2.309(2); 2.194(2)	164.92
$[MnF_3(H_2O)(L_4)]\cdot 2H_2O$ (**4**)	2.216(8), 2.146(7)	166.67
$[MnF_3(H_2O)(L_5)]\cdot 0.5MeOH$ (**5**)	2.246(3); 2.171(3)	168.60
$[MnF_3(H_2O)(L_6)]$ (**6**)	2.260(7); 2.153(7)	167.25

Table 2 X-ray crystallographic data obtained from complexes **1′ -4**

	1′·$2H_2O$	**2′**	**3**	**4**·$2H_2O$
Formula[a]	$C_{10}H_{14}N_2O_3F_3Mn_1$	$C_{12}H_{10}N_2O_1F_3Mn_1$	$C_{11}H_{12}N_2O_1F_3Mn_1$	$C_{12}H_{14}N_2O_3F_3Mn_1$
M_W	322.17	310.16	300.17	346.19
Crystal System	Monoclinic	Monoclinic	Monoclinic	Triclinic
Space group	$P2_1/n$	$P2_1/c$	$P2_1/c$	P-1
a/Å	9.0453(2)	8.3759(17)	8.3482(4)	6.8782(5)
b/Å	7.4043(2)	7.2941(15)	7.4997(3)	10.3111(14)
c/Å	19.4455(4)	19.268(4)	18.7579(10)	10.6165(19)
α/°	90	90	90	73.723(15)
β/°	95.425(2)	101.83(3)	102.664(4)	86.860(12)
γ/°	90	90	90	85.570(9)
V/Å^3	1296.51(5)	1152.2(4)	1145.84(10)	720.17(17)
Z	4	4	4	2
T/K	150(2)	150(2)	150(2)	150(2)
λ[b]/Å	0.71073	0.71073	0.71073	0.71073
D_c/g cm^{-3}	1.651	1.788	1.740	1.596
μ(Mo-Ka)/ mm^{-1}	1.060	1.177	1.180	0.960
Meas./indep.(R_{int}) refl.	3156/2390 (0.0633)	2105/1840 (0.0287)	2089/1933 (0.0195)	2649/2065(0.0534)
Restraints, Parameters	9, 196	0, 180	0, 172	0, 196
wR2 (all data)	0.0879	0.0931	0.0585	0.3463
$R1^{d,e}$	0.0564	0.0360	0.0221	0.1208
Goodness of fit on F^2	1.047	1.082	1.075	1.116

[a] Includes guest molecules. [b] Mo-Kα radiation, graphite monochromator. [c] $wR2 = [\Sigma w(|F_o^2| - |F_c^2|)^2 / \Sigma w|F_o^2|^2]^{1/2}$. [d] For observed data. [e] $R1 = \Sigma||F_o| - |F_c|| / \Sigma|F_o|$.

Table 3. X-ray crystallographic data obtained from complexes **5** and **6.**

	5·0.5MeOH	**6**
Formula[a]	$C_{12.5}H_{14.5}N_2O_{1.5}F_3Mn_1$	$C_{12}H_9N_2O_1Cl_1F_3Mn_1$
M_W	328.70	344.60
Crystal System	Monoclinic	Orthorhombic
Space group	I2/a	Pbca
a/Å	16.4291(7)	7.3151(5)
b/Å	7.6236(4)	16.5375(14)
c/Å	23.0374(14)	20.773(2)
α/°	90	90
β/°	102.176(5)	90
γ/°	90	90
V/Å^3	2820.5(3)	2513.0(4)
Z	8	8
T/K	150(2)	150(2)
λ[b]/Å	0.71073	0.71073
D_c/g cm^{-3}	1.548	1.822
μ(Mo-Ka)/ mm^{-1}	0.969	1.295
Meas./indep.(R_{int}) refl.	2573/2226 (0.03233)	2297/1224(0.2124)
Restraints, Parameters	0, 189	0, 186
wR2 (all data)	0.1108	0.2065
$R1^{d,e}$	0.0453	0.0812
Goodness of fit on F^2	1.183	1.042

[a] Includes guest molecules. [b] Mo-Kα radiation, graphite monochromator. [c] $wR2 = [\Sigma w(|F_o^2| - |F_c^2|)^2 / \Sigma w|F_o^2|^2]^{1/2}$. [d] For observed data. [e] $R1 = \Sigma||F_o| - |F_c|| / \Sigma|F_o|$.

Magnetic susceptibility measurements

Dc magnetic susceptibility measurements were performed on powdered microcrystalline samples of **1′-6** in an applied magnetic field of 0.1 T and in the temperature range 300 to 5 K. The results are plotted as the $\chi_M T$ products versus *T* in the

insets of Figure 4 and Figures S3 and S4. The high temperature $\chi_M T$ values obtained range from 2.84 (in **2'**) to 3.29 (in **3**) cm^3 K mol^{-1} and are very close to that expected (3.00 cm^3 K mol^{-1} for g = 2.00) for a single, high-spin, d^4 Mn(III) ion. The values decrease gradually before dropping more rapidly at lower temperatures (~10 K). This behaviour can be assigned to the combination of extensive [and rather complicated] intermolecular interactions observed in the crystal structures of **1′**-**6** and zero-field splitting effects. The T = 5 K χ_MT products all lie in the range 1.94 (**2'**) to 2.57 (**5**) cm^3 K mol^{-1}, somewhat lower than that expected from an isolated, isotropic S = 2 ion (3.00 cm^3 K mol^{-1}, g = 2.00). In order to determine the single-ion axial anisotropy parameter for the Mn(III) centres in **1′**-**6** variable-temperature-variable-field dc magnetisation (M) experiments were performed in the 2.0–7.0 K and 0.5–7.0 T temperature and magnetic field ranges. The experimental data are presented in Figures 4, S3 and S4. The data were numerically fitted by use of the simplex algorithm[20] to the spin-Hamiltonian below, by numerical diagonalisation of the full spin-Hamiltonian matrix.

$$\hat{H} = \sum_{i=1} \{\mu_B \vec{B} g \hat{S}_i + D[\hat{S}^2_{z,i} - S_i(S_i+1)/3]\}$$

Here, D is the uniaxial anisotropy and $S_{Mn(III)}$ = 2 the total spin of the Mn(III) ion. The best fit $D_{Mn(III)}$ parameters were (cm^{-1}): -3.97 (**1'**), -3.01 (**2'**), -3.10 (**3**), -3.90 (**4**), -4.02 (**5**) and -3.97 (**6**) (Table 3). These ZFS parameters were then employed to fit the corresponding magnetic susceptibility data, which also required use of a mean field term (zJ') affording values of -0.55 K (**1'**); -1.33 K (**2'**); -1.00 K (**3**); -0.25 K (**4**); +0.07 K (**5**); -1.11 K (**6**).

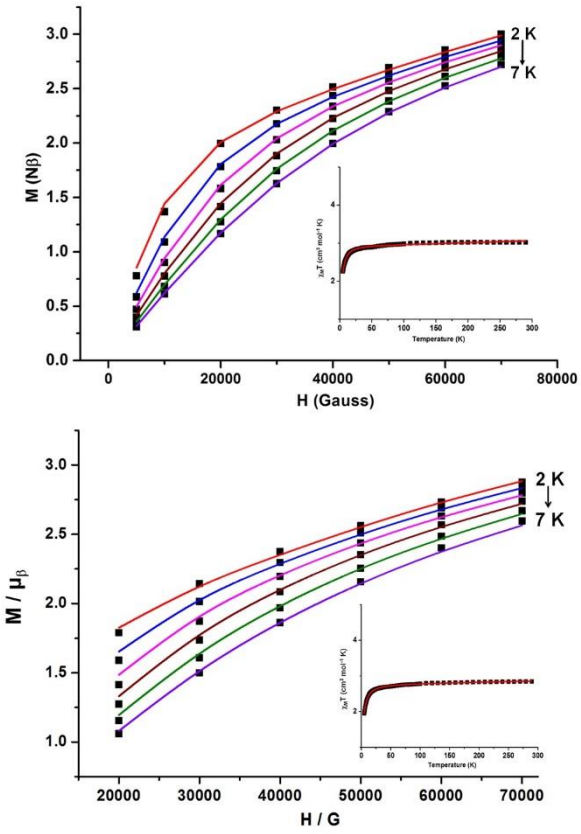

Figure 4. Plots of magnetisation (M / μ_B) versus Field (H / G) and (insets) magnetic susceptibility ($\chi_M T$ / cm^3 K mol^{-1}) versus temperature (T / K) obtained from polycrystalline samples of **1'** (top) and **2'** (bottom). The solid lines represent the best-fit to the data. See main text and Table 4 for details.

MF / HF-EPR Spectroscopy

The magnitude of the D tensor obtained for **1′-6** each lie on the upper limit of standard W-band spectrometers and so multi-frequency / high field EPR was employed here. Powdered and pelletised samples of **1'**, **2'**, **4** and **5** were measured at several frequencies ranging from 220 GHz to 575 GHz and at both 15 and 5 K (Figures 5-7 and S5-8). In all spectra, a signal at g = 2 (at 7.9 T for 220.8 GHz and 11.8 T at 331.2 GHz) is observed with an increasing intensity as the temperature is increased and is tentatively assigned to a Mn(II) impurity. For all frequencies, several signals are recorded whose intensities change markedly with temperature. All spectra exhibit complicated fine structure, as expected for complexes with uniaxial anisotropies of several wavenumbers, which forbid any simple preliminary analysis. Satisfactory simulations of the spectra were obtained for all four complexes giving rise to the following sets of parameters: D = -4.25(3) cm^{-1}, E = 0.49(3) cm^{-1}, $g_x = g_y$ = 1.99(6) and g_z = 2.00(5) (**1'**); D = -4.03(5) cm^{-1}, E = 0.18(2) cm^{-1}, $g_x = g_y$ = 1.96(5) and g_z = 1.98(4) (**2'**); D = -3.90(3) cm^{-1}, E = 1.20(2) cm^{-1}, $g_x = g_y$ = 1.98(6) and g_z = 2.00(5) (**4**) and D = -4.04(6) cm^{-1}, E = 0.22(3) cm^{-1}, $g_x = g_y$ = 2.00(7) and g_z = 2.00(6) (**5**); which are comparable to those obtained from magnetisation measurements (Table 4). It should be noted here that accuracy in ascertaining g-values is severely hampered due to the masking effect of the large $|D|$ terms associated with each complex. As shown in Figures 5-7 (and S5-S8), the resonance positions in the experimental spectra are rather well reproduced in comparison to their corresponding simulated spectra, however their relative intensities within each spectrum are less satisfactorily reproduced. This less than ideal intensity reproduction is likely attributed to commonly observed torqueing effects; that are minimised (although not eradicated) through sample pelletisation, as is the case in this work.

For all complexes, the *z* component of their M = -2 → -1 transition are observed in the spectra recorded at the highest frequencies; corresponding to an intense feature close to 3.5 T (at 460 GHz) and 7.5 T (at 575 GHz) at 5 K, whose intensity decreases when the temperature is increased. Similarly, at 220.8 GHz, the *x* and *y* components of the M = -2 → -1 transition are clearly observed in the high field part of the spectra, with the same temperature behaviour. More specifically, the *y* component appears close to 13.5 T for complexes **1'**, **2'** and **5** (Fig. 5 and S7) and at 9.3 T for the more rhombic complex **4** (Fig. 7). The *x* component is observed only for complexes **2'** and **5** at 15.5 and 15.3 T respectively. For complexes **1'** and **4** this resonance is expected at fields lying outside the range of our superconducting magnet (> 16 T). For all complexes except **2'** (where the S/N does not allow confident assignment), signals associated with the M = -1 → 0 transition are also observed, especially in the spectra recorded at 331.2 GHz. The z component is found at 8.7 T (**1'** and **5**) or 9.2 T (**4**), while the *x* component resonated close to 12 T for both **1'** and **5** and at 14.6 T for **4**. The corresponding *y* component signals are observed at 9.3 T (**1'**), 8.8 T (**4**) and 10.4 T (**5**). The other recurrent features associated with allowed transitions are the *x* and *y* components of the M = 0 → +1 transition. For instance at 460 GHz, the *x* component is found at 13.0 T (**1'**), 13.7 T (**2'**), 12.6 T (**4**) and 13.2 T (**5**), whereas the *y* component is found at 13.6 T (**1'** and **5**), 13.9 T (**2'**) and 14.1 T (**4**). As shown in Figures 6, 7 and S7, the close to zero field signal observed in the 331.2 GHz spectra of **1'**, **2'** and **5** are assigned to the *z* component of the 'forbidden' transition M_{ZFS} = +2 → -1 (using the ZFS labelling of the energy levels). Such a signal is absent for complex **4**, where a quasi-rhombic (|*E*/*D*| ~ 0.31) energy diagram holds.

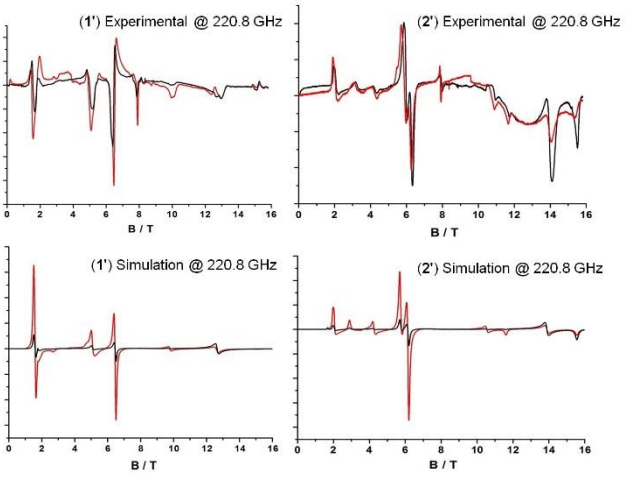

Figure 5. Experimental and simulated MF / HF-EPR spectra obtained on polycrystalline sample pellets of $[MnF_3(H_2O)(L_1)]\cdot 2H_2O$ (**1'**) and $[MnF_3(H_2O)(L_1)]$ (**2'**), carried out and simulated at a frequency of 220.8 GHz and temperatures of 15 K (red line) and 5 K (black line).

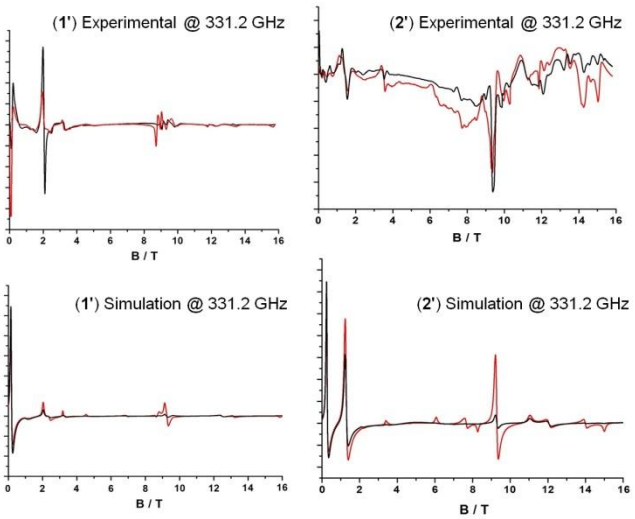

Figure 6. Experimental and simulated MF / HF-EPR spectra obtained on polycrystalline sample pellets of $[MnF_3(H_2O)(L_1)]\cdot 2H_2O$ (**1'**) and $[MnF_3(H_2O)(L_1)]$ (**2'**), carried out and simulated at a frequency of 331.2 GHz and temperatures of 15 K (red line) and 5 K (black line).

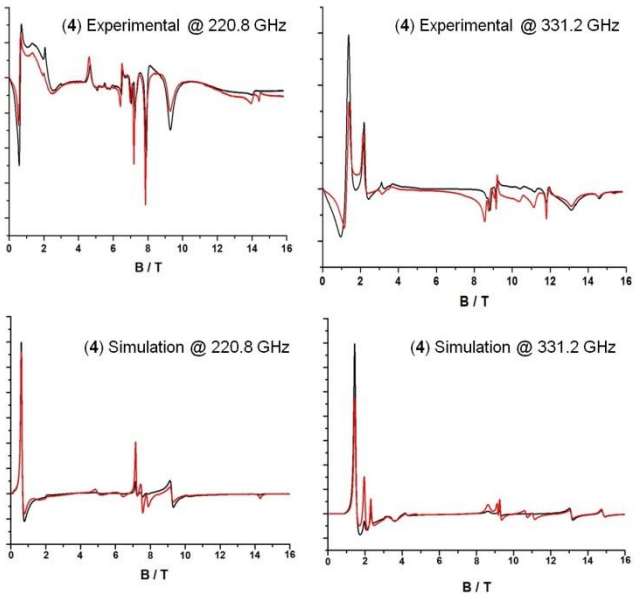

Figure 7. Experimental and simulated MF / HF-EPR spectra obtained on a polycrystalline sample pellets of $[MnF_3(H_2O)(L_4)]\cdot 2H_2O$ (**4**), carried out and simulated at frequencies of 220.8 and 331.2 GHz respectively and temperatures of 15 K (red line) and 5 K (black line).

Table 4. Anisotropic magnetic parameters obtained from **1′**-**6** using magnetisation versus field (M vs H) and MF / HF-EPR measurements.
Key: - = not measured.

M vs H studies			MF / HF-EPR studies				
Complex	**g-value**	**D (cm^{-1})**	**g_x**	**g_y**	**g_z**	**D (cm^{-1})**	**E (cm^{-1})**
$[MnF_3(H_2O)(L_1)]\cdot 2H_2O$ (**1′**)	2.0	-3.97	1.99(6)	1.99(6)	2.00(5)	-4.25(3)	0.49(3)
$[MnF_3(H_2O)(L_2)]$ (**2′**)	2.0	-3.01	1.96(5)	1.96(5)	1.98(4)	-4.03(5)	0.18(2)
$[MnF_3(H_2O)(L_3)]$ (**3**)	2.0	-3.10	-	-	-	-	-
$[MnF_3(H_2O)(L_4)]\cdot 2H_2O$ (**4**)	2.0	-3.90	1.98(6)	1.98(6)	2.00(5)	-3.90(3)	1.20(2)
$[MnF_3(H_2O)(L_5)]\cdot 0.5MeOH$ (**5**)	2.0	-4.02	2.00(7)	2.00(7)	2.00)(6)	-4.04(6)	0.22(3)
$[MnF_3(H_2O)(L_6)]$ (**6**)	2.0	-3.97	-	-	-	-	-

Complexes **1′**-**6** add to a 600+ long list of reported monomeric Mn(III) complexes although only a small percentage (~5%) of these publications come with significant magnetic elucidation. For convenience, these complexes along with their various spin Hamiltonian parameters (*i.e. g*, *D* and *E* tensors) are given in Table S6. The spin Hamiltonian data extracted here are comparable to literature values, including the structurally related complex [Mn(III)F_3(terpy)] (D = -3.82 cm^{-1}, E = 0.75 cm^{-1}, g_x = 1.97(2), g_y = 2.04(1) and g_z = 1.96(1)); where terpy = 2,2':6',2''-terpyridine (see Table S6 for more information).[21] The simulation of complex **4** requires a significantly larger rhombic term (E = 1.20(2) cm^{-1}) when compared to its siblings (ranging from 0.18(2) cm^{-1} (in **2'**) to 0.49(3) in **1'**) and may be attributed to its lower symmetry highlighted by its less pronounded axial elongation, with distances of Mn1-N1 (2.216(8)) and Mn1-O1 (2.146(7)) when compared to **1'** (Mn1-N1 = 2.220(2), Mn1-O1 = 2.176(2)), **2'** ((Mn1-N1 = 2.261(2), Mn1-O1 = 2.166(2)) and **5** (Mn1-N1 = 2.246(3), Mn1-O1 = 2.171(3)) (see Table 1). Another contributing factor may be the lower symmetry crystallisation of **4** (triclinic, *P*-1) when compared to complexes **1'** and **2'** (monoclinic $P2_1/n$ and $P2_1/c$ respectively), although it should be noted that complex **5** also crystallises in a monoclinic space group (*I*2/a).

Raman Studies

Solid state Raman spectra were obtained from 1.5% w/w dispersions in KBr solid matrices of complexes **1′**-**6**, ligands L_1-L_6 and MnF_3 as purchased (see experimental section for details), while FT-IR spectra were also obtained from polycrystalline samples of **1′**-**6**. All data were normalised and baseline corrected using standard methods unless otherwise stated. The experimental Raman spectrum of MnF_3 deviates from the published literature values (283, 513 and 651 cm^{-1} in ref. [22] and 530, 619 and 655 cm^{-1} in ref. [23]). The peaks at 655 (and 651 cm^{-1}) and at 619 and 530 cm^{-1} were tentatively attributed to Mn-F and Mn-F-Mn bridge stretching modes, respectively.[23] When the MnF_3 / KBr matrix was prepared in this work the spectrum obtained exhibits prominent peaks at 262 (broad), 420-491 (a set of six bands), a strong peak at 574 with a shoulder at 595(sh) and a peak at 625 cm^{-1} (Fig. S10). We attribute these differences to the hygroscopic nature of the MnF_3 starting material, leading to the formation of the $MnF_3.3H_2O$ hydrate (of which there are two polymorphs). [24] Indeed, peaks in the 300-400 cm^{-1} region of our MnF_3 spectrum correspond to Mn-OH_2 stretches as observed in the literature.[25]

The weak band at 625 cm^{-1} is attributed to MnF_3, however since it is ~1/3rd as intense as the 574 cm^{-1} band (which can be attributed to the terminal Mn-F stretching of the various octahedral Mn(III) species), it means that it is present in low concentration. The 491 cm^{-1} band is assigned to the Mn-F-Mn bridge stretching mode. The Raman spectra of **1′**-**6** corroborate these findings with each sample exhibiting peaks in these regions (*i.e.* 244, 481 and 582 cm^{-1} in **1′** and 276, 482, 574 cm^{-1} in **2′**) (Figures 8, 9, S10 and S14). Since rigorous moisture control was not implemented during storage of the anhydrous MnF_3, we cannot be certain which octahedral species are present in the MnF_3 starting material. Acquisition of the Raman spectra of pure anhydrous MnF_3 by this KBr disc method would have required a much more arduous procedure, which was not necessary here, it was more important to look at the starting material as used during the synthesis of **1'-6**. Moreover, the KBr method was necessary for these darkly coloured complexes as many were burnt due to excessive absorption of excitation light; a common problem with coloured compounds during Raman analysis.

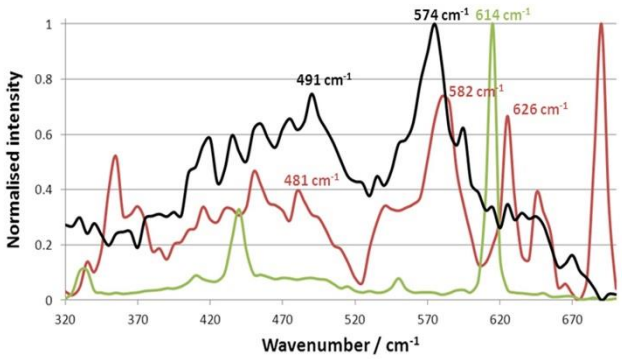

Figure 8. Raman spectra in the 320-700 cm^{-1} region obtained from a crystalline sample of [Mn(III)F_3(H_2O)(L_1)]·$2H_2O$ (**1′**) (red line), 2,2'-bipyridyl (green line) and a MnF_3·$3H_2O$ / KBr mixture (black line).

Similarities between the Raman spectra of **1′** and 2,2'-Bipyridyl (L_1) can be seen in Figures 8, S9 and S12 and pertinent bands are also tabulated in Tables S2 and S3. Castellucci and co-workers made reliable assignments of the internal Raman modes of 2,2'-bipyridyl and designated peaks at 616, 1056 and 1308 cm^{-1} to an in-plane ring deformation, ring-ring stretching and a C-H deformation respectively,[26] while other research groups have described similar results.[27],[28] These figures compare well with our experimental figures of 614, 1046 and 1301 cm^{-1} for 2,2'-bipyridyl. Related peaks are present in the spectrum of complex **1′** at 626, 1059 and 1311 cm^{-1}. Likewise, Figure 9 highlights the similarities between the Raman spectra of **2′** and 1,10'-phenanthroline (L_2). More specifically, peaks at 410, 710, 1035, 1295, 1406 and 1445 cm^{-1} are the most intense bands observed in the Raman spectrum of L_2, which correlate with literature values as shown in Table S4. These bands are due to in-plane modes (A_1).[29],[30]

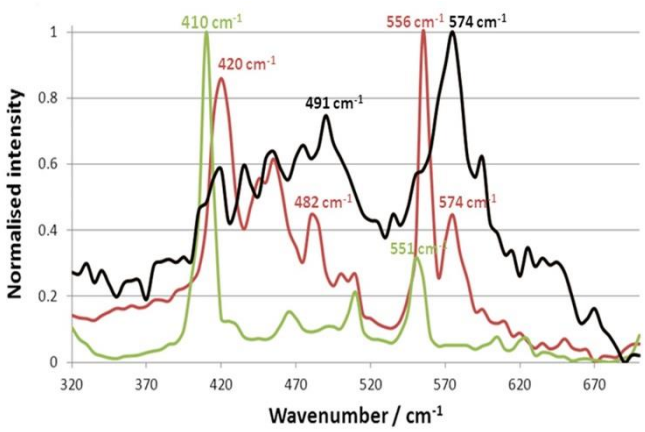

Figure 9. Raman spectra in the 320-700 cm^{-1} region obtained from a crystalline sample of $[Mn(III)F_3(H_2O)(L_2)]$ (**2′**) (red line), 1,10-Phenanthroline (green line) and a $MnF_3{\cdot}3H_2O$ / KBr mixture (black line).

FT-IR and Raman spectra were obtained from complexes **3**-**6** along with their corresponding ligands (L_3-L_6). Overlays of these plots are given in the supplementary information (Figures S17-S25) and show similar and consistent trends with the corresponding data obtained from complexes **1′** and **2′**. We were unable to locate literature values for the Raman bands associated with 6-methyl-2,2'-dipyridyl (L_3), 4,4'-dimethyl,2,2'-dipyridyl (L_4), 5,5-dimethyl-2,2'-dipyridyl (L_5) and 5-chloro-1-10-phenanthroline (L_6), however our data on L_3-L_6 were found to be consistent with data from 2,2'-bipyridyl (L_1 *cf.* L_3-L_5) and 1,10'-phenanthroline (L_2 *cf.* L_6), respectively.

Conclusions

We have demonstrated a new and facile synthetic route to a family of Mn(III) monomers with general formula $[MnF_3(H_2O)(L_{1\text{-}6})]$. Magnetic susceptibility and magnetisation studies along with MF / HF-EPR spectroscopy were successfully employed to elucidate their *D*-tensor parameters, which are in line with each other and commensurate with literature values. Raman spectroscopy was also used to look at Mn-F vibrational modes and subsequently compared to literature values. Work is currently underway on using **1′**-**6** as presursors to discrete polymetallic cages and as building blocks to 1-3D extended architectures using self-assembly routes. Investigations into their potential catalytic ability are also ongoing.

Experimental Section

All reagents and solvents were purchased commercially and used as supplied. Take caution when handling MnF_3 and heating solvent solutions. All manipulations were carried out in a fumehood and protective clothing was used throughout.

General synthesis of $[Mn(III)F_3(H_2O)(L_{1\text{-}6})]$

$Mn(III)F_3$ (0.5 g, 4.46 mmol) and one equivalent of ligand 'L_x' were dissolved in 25 cm^3 MeOH. The subsequent methanolic solution was warmed (with rapid stirring) on a heating mantle in a fumehood until the solution was simmering (~50°C). The solution was removed from the heat source using forceps as soon as a dark red colour was obtained. The resulting solution was then filtered upon cooling and X-ray quality crystals of **1'-6** were obtained upon slow evaporation of their mother liquors. Full details are available in the ESI.

Single crystal X-ray structure determination

The structures of **1′**-**6** were collected on an Xcalibur S single crystal diffractometer (Oxford Diffraction) using an enhanced Mo source. Each data reduction was carried out on the CrysAlisPro software package. The structures were solved by direct methods (SHELXS-97)[31] and refined by full matrix least squares using SHELXL-97.[32] SHELX operations were automated using the OSCAIL software package.[33] All non-hydrogen atoms were refined as anisotropic. The hydrogen atoms belonging to the bound water molecules in **1′**-**6** were located in the difference map. All other hydrogens were placed in calculated positions. The two waters of crystallisation in **4** were refined as anisotropic. The MeOH (labelled C13-O2) solvent molecule in **5** was modelled as disordered over two sites with 50:50 occupancy, while its associated proton (H2) was placed in a calculated position lying along an appropriate direction at a distance of 1.849 Å from F3. CCDC numbers: 1489265 (**1'**) – 1489270 (**6**).

MF / HF-EPR spectroscopy

MF / HF-EPR measurements were performed on a multi-frequency spectrometer[34] operating in a double-pass configuration. A 110 GHz frequency source (Virginia Diodes Inc.) is multiplied by a doubler or a tripler to obtain 221 or 331 GHz, respectively. The 460 and 575 GHz spectra were obtained using a 115 GHz Gunn oscillator (Radiometer Physics GmbH) together with a quadrupler or a quintupler. The detection is performed with a hot electron InSb bolometer (QMC Instruments). The exciting light is propagated with a Quasi-Optical set-up (Thomas Keating) outside the cryostat and with the help of a corrugated waveguide inside it. The main magnetic field is supplied by a 16 T superconducting magnet associated to a VTI (Cryogenic). The measurements were done on

powdered samples pressed into pellets in order to limit torqueing effects. Calculated spectra were obtained with the SIM program[35] from H. Weihe (Univ. of Copenhagen).

Other measurements

Elemental analyses were carried out at the School of Chemistry, NUI Galway. Magnetic susceptibility measurements were obtained using a Quantum Design SQUID magnetometer in an applied field of 1000 G. Diamagnetic corrections were estimated from Pascal's constants. All measured complexes were set in eicosane to avoid torqueing of the crystallites. All magnetic samples were collected as single-crystalline products and analysed using microanalysis and IR measurements prior to their magnetic assessment. If necessary, phase purity between cross-batches were validated using unit cell checks and IR measurements.

Infra-red spectra were recorded on a Perkin Elmer FT-IR *Spectrum One* spectrometer equipped with a Universal ATR Sampling accessory. Raman measurements were recorded at room temperature using a Raman WORKSTATION™ Analyzer with PhAT imaging probe (Kaiser Optical Systems, Inc.) with 785 nm excitation. An exposure time of 10 × 8 seconds was used and spectra were collected from 250 to 4000 cm^{-1} (at a resolution of 5 cm^{-1}). Raman spectra of the coloured complexes **1′**-**6** were collected from a solid dispersion (approximately 1.5% by weight of complex) in dry KBr which was pressed into a disk using a hydraulic press and a 13 mm die set. This was done to minimise sample burning due to excessive absorption of excitation light. All data were normalised to the peak of maximum intensity and baseline corrected using standard methods.

Acknowledgements

The authors would like to thank the IRSCET Embark Fellowship (EH) and the EPRSC (SS and EKB) for funding. We would also like to thank the EPSRC National EPR Service for their assistance (EJLM, DC).

Keywords: Molecular Magnetism • Electron Paramagnetic Resonance • Zero-field splitting • $Mn(III)F_3$ • D-tensor.

[1] Commercially available salts include $Mn(acac)_3$ (where acac = acetylacetonate), Mn_2O_3 and $Mn(OAc)_3{\cdot}2H_2O$ (although in reality the latter has the trinuclear formula $[Mn(III)_3O(OAc)_6(solvent)_3](OAc)$).

[2] For a suitable review on the role of manganese(III) acetate in organic synthesis see: M. Mondal, U. Bora. *RSC Advances*. **2013**, 3, 18716-18754.

[3] B. B. Snider. *Chem. Rev*., **1996**, 96, 339-363.

[4] a) E. J. Larson, V. L. Pecoraro. *Manganese Redox Enzymes*, ed. V. L. Pecoraro, VCH Publisher, Inc., New York, **1992**, p. 1. b) M. J. Gunter, R. Turner. *Coord. Chem. Rev*., **1991**, 108, 115. c) A. Galstyan, A. Robertazzi, and E. W. Knapp. *J. Am. Chem. Soc*. **2012**, 134, 7442-7449.

[5] a) S. P. H. Mee, V. Lee, J. E. Baldwin. *Angew. Chem. Int. Ed*., **2004**, 43, 1132-1136. b) S. P. H. Mee, V. Lee, J. E. Baldwin. *Chem. Eur. J*. **2005**, 11, 3294-3308. c) M. Herve, G. Lefevre, E. A. Mitchell, B. U. W. Maes, A. Jutand. *Chem. Eur. J*. **2015**, 21, 18401-18406.

[6] a) C. Amatore, A. Jutand, G. Le Duc. *Angew. Chem. Int. Ed.,* **2012**, 51, 1379-1382. b) C. Amatore, G. Le Duc, A. Jutand. *Chem. Eur. J*. **2013**, 19, 10082-10093.

[7] C. Amatore, L. Grimaud, G. Le Duc, A. Jutand. *Angew. Chem. Int. Ed*. **2014**, 53, 6982-6985.

[8] a) *Molecular Magnetism*, O. Kahn. Wiley Publishing. **1993**, b) *Molecular Nanomagnets*, D. Gatteschi, R. Sessoli and J. Villain. Oxford Press., **2006**. c) *Molecular Cluster Magnets.,* World Science Series in Nanoscience and Nanotechnology.-Vol. 3. R. E. P. Winpenny. World Scientific Publishing*.,* **2012**.

[9] G. Aromi, E. K. Brechin. *Struct. and Bonding*. Springer. Chapter 1. p.1 - 67.

[10] N. V. Gerbeleu, Yu. T. Struchkov, G. A. Timco, A. S. Batsanov, K. M. Indrichan, G. A. Popovich, *Dokl. Akad. Nauk. SSSR*, **1990**, 313, 1459.

[11] M. L. Baker, G. A. Timco, S. Piligkos, J. M. Mathieson, H. Mutka, F. Tuna, P. Kozlowski, M. Antkowiak, T. Guidi, T. Gupta, H. Rath, R. J. Woolfson, G. Kamieniarz, R. G. Pritchard, H. Weihe, L. Cronin, G. Rajarman, D. Collison, E. J. L. McInnes, R. E. P. Winpenny. *P. Nas. Acac. Sci.,* **2012**, 109(47), 19113-19118.

[12] E. J. L. McInnes, S. Piligkos, G. A. Timco, R. E. P. Winpenny. *Coord. Chem. Rev*., **2005**, 249, 2577-2590.

[13] F. A. Larsen, E. J. L. McInnes, H. El Mkami, J. Overgaard, S. Piligkos, G. Rajaraman, E. Rentschler, A. A. Smith, G. M. Smith, V. Boote, M. Jennings, G. A. Timco, R. E. P. Winpenny. *Angew. Chem. Int. Ed*., **2003**, 42, 101-105.

[14] a) S. A. Oschsenbein, F. Tuna, M. Rancan, R. S. G. Davies, C. A. Muryn, O. Waldmann, R. Bircher, A. Sieber, G. Carver, H. Mutka, F. Fernandez-Alonso, A. Podlesnyak, L. P. Englehardt, G. A. Timco, H. U. Güdel, R. E. P. Winpenny. *Chem. Eur. J.* **2008**, 14, 5144-5158. b) L. P. Englehardt, C. A. Muryn, R. G. Pritchard, G. A. Timco, F. Tuna, R. E. P. Winpenny. *Angew. Chem. Int. Ed.,* **2008**, 47, 924-927. c) F. A. Larsen, J. Overgaard, S. Parsons,

E. Rentschler, A. A. Smith, G. A. Timco, R. E. P. Winpenny. *Angew. Chem. Int. Ed.,* **2003**, 42, 5978-5981.

[15] K. S. Pedersen, G. Lorusso, J. J. Morales, T. Weyhermüller, S. Piligkos, S. K. Singh, D. Larsen, N. Schau-Magnussen, G. Rajaraman, M. Evangelisti, J. Bendix. *Angew. Chem. Int. Ed*. **2014**, 53, 2394-2397.

[16] M. N. Bhattacharjee, M. K. Chaudhuri, R. N. Dutta, Purkayatsha., *Inorg. Chem.,* **1989**, 28, 3747 – 3752.

[17] P. Núñez, C. Elias, J. Fuentes, X. Solans, A. Tressaud, M. C. Marco de Lucas, F. Rodrigues., *Dalton. Trans.,* **1997**, 4335-4340.

[18] A. R. Biju, M. V. Rajasekharan. *J. Mol. Struct.* **2008**, 875, 456-461.

[19] a) L. F. Jones, J. Raftery, S. J. Teat, D. Collison, E. K. Brechin. *Polyhedron*, **2005**, 24, 2443. b) L. F. Jones, G. Rajaraman, J. Brockman, M. Murugesu, E. Carolina Sañudo, J. Raftery, S. J. Teat, W. Wernsdorfer, G. Christou, E. K. Brechin, D. Collison. *Chem. Eur. J*., **2004**, 10, 5180-5194. c) L. F. Jones, E. K. Brechin, D. Collison, J. Raftery, S. J. Teat. *Inorg. Chem.,* **2003**, 42, 6971-6973. d) L. F. Jones, E. K. Brechin, D. Collison, A. Harrison, S. J. Teat, W. Wernsdorfer, *Chem. Commun.,* **2002**, 24, 2974-2975.

[20] W. H. Press, S. A. Teukolsky, W. T. Vetterling, B. P. Flannery, *"Numerical Recipes in C: The Art of Scientific Computing"*. Second Edition, Cambridge, Cambridge University Press, **1992**.

[21] C. Mantel, A. K. Hassan, J. Pécaut, A. Deronzier, M.-N Collomb, C. A. Duboc-Toia,. *J. Am. Chem. Soc*., **2003**, 125 (40), 12337-12344.

[22] Z. Mazej, *Journal of Fluorine Chemistry* **2002**, *114*, 75-80.

[23] a) W. Sawodny, K. M. Rau. *J. Fluor. Chem*., **1993**, 61, 111-116. b) M. Adelhelm, E. Jacob. *J. Fluor. Chem*., **1991**, 54, 21.

[24] M. Molinier, W. Massa. *J. Fluor. Chem.,* **1992**, 57, 139-146.

[25] A. Cua, D. H. Stewart, M. J. Reifler, G. W. Brudvig, D. F. Bocian. *J. Am. Chem. Soc*., **2000**, 122, 2069-2077.

[26] E. Castellucci, L. Angeloni, N. Neto, G. Sbrana, *Chemical Physics,* **1979**, 43, 365-373S.

[27] Umapathy, G. Lee-Son, R. E. Hester, *Journal of Molecular Structure* **1989**, 194, 107-116.

[28] M. Kim, K. Itoh, *Journal of electroanalytical chemistry and interfacial electrochemistry* **1985**, 188, 137-151.

[29] M. Reiher, G. Brehm, S. Schneider, *The Journal of Physical Chemistry A* **2004**, 108, 734-742.

[30] D. A. Thornton, G. M. Watkins, *Spectrochimica Acta Part A: Molecular Spectroscopy* **1991**, 47, 1085-1096.

[31] G. M. Sheldrick, *Acta. Crystallogr., Sect. A: Found. Crystallogr.,* **1990**, A46, 467.

[32] G. M. Sheldrick, SHELXL-97, A computer programme for crystal structure determination, University of Gottingen, **1997**.

[33] P. McArdle, P. Daly, D. Cunningham, *J. Appl. Crystallogr*., **2002**, 35, 378.

[34] A. L. Barra, A. K. Hassan, A. Janoschka, C. L. Schmidt, V. Schünemann, *Appl. Magn. Reson.*, **2006**, 30, 385-397.

[35] J. Glerup, H. Weihe, *Inorg. Chem.*, **1997**, 36, 2816-2819.

Entry for the Table of Contents (Please choose one layout)

Layout 1:

FULL PAPER

We report a rapid and facile synthetic route to the synthesis of a family of Mn(III) monomers of general formula $[Mn(III)F_3(H_2O)(L_{1\text{-}6})]$. Magnetic susceptibility and magnetisation experiments along with multi-frequency / high-field EPR were employed to elucidate anisotropic *D* tensors. The terminal Mn-F vibrational stretches have been probed using Raman spectroscopy.

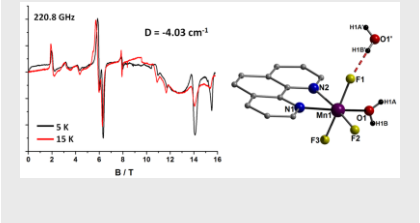

MF / HF-EPR

Edel Houton, Brian Kelly, Sergio Sanz, Eric J. L. McInnes, David Collison, Euan K. Brechin, Anne-Laure Barra, Alan G. Ryder and Leigh F. Jones.

Page No. – Page No.

A Facile Synthetic Route to a Family of Mn(III) Monomers and their Structural, Magnetic and Spectroscopic Studies